NUMERICAL SIMULATIONS OF DUCTILE FAILURE IN EXTRUDED ALUMINIUM ALLOYS USING A COUPLED MODEL OF ELASTO-PLASTICITY AND DAMAGE

O.-G. Lademo, O.S. Hopperstad, T. Berstad and M. Langseth*
Structural Impact Laboratory – SIMLab
Department of Structural Engineering
Norwegian University of Science and Technology
N-7491 Trondheim, Norway
E-mail: odd.hopperstad@bygg.ntnu.no

**Currently at SINTEF Materials Technology*
Fracture Mechanics and Materials Testing
N-7456 Trondheim, Norway

Abstract

A test programme has been carried out to establish the mechanical properties of three extruded aluminium alloys. The investigated alloys exhibited significant anisotropy in strength, plastic flow and ductility. The anisotropy is mainly due to crystallographic texture, and an anisotropic yield criterion is needed to describe the mechanical behaviour. Several yield criteria were evaluated against the experimental data. The yield criterion Yld96 proposed by Barlat and co-workers was found to be superior with respect to accuracy for the actual aluminium alloys. In an attempt to model ductile failure of the investigated materials, a coupled model of elasto-plasticity and ductile damage was implemented in LS-DYNA for plane stress analysis with co-rotational shell elements. The material model combines the anisotropic yield criterion Yld96 with the associated flow rule, isotropic strain hardening and isotropic damage. The parameters defining the yield criterion and the strain hardening were determined from tensile tests and pure bending tests, while the damage parameters were identified using inverse modelling of tensile tests performed with purpose-made specimens. A series of biaxial tensile tests was also completed, and the results from these tests were used in an attempt to evaluate the constitutive model.

Introduction

In the recent years, increasing concern for economy, environment and functionality has led to the use of aluminium alloys in load-carrying structures and safety components of cars. The motivation is manifold. The use of aluminium may reduce the weight of the car considerably, and thus bring down the energy consumption and emissions to the environment. Re-cycling of aluminium is environmentally and economically profitable. Extruded aluminium parts open up for novel concepts in car design. One such concept is the aluminium space frame. The space frame consists of thin-walled extrusions formed by bending and joined at nodes into a three-dimensional framed structure.

In the design of space frames and safety components of aluminium alloys, such as bumper beams and crash boxes, finite element analysis is used to predict the behaviour of the extrusions during cold forming and to assess the crashworthiness of the final part. The reliability of the finite element analyses depends strongly on the material models used to describe the mechanical properties of the aluminium alloys. Extruded aluminium alloys often exhibit complex stress-strain behaviours, and improved and validated material models are indeed required for increased predictability. Since the material models are aimed at large-scale simulations in an industrial context, efficiency and easy parameter identification are important aspects in addition to accuracy. In this study, a coupled model of elasto-plasticity and ductile damage is implemented in LS-DYNA [1]. The model parameters are determined for the extruded aluminium alloy AA7108, using an identification method based on simple tensile and bending tests. The material model is then evaluated against data from more complex biaxial tensile tests on cruciform specimens. The main equations of the constitutive model and some results are presented in this paper.

Coupled model of elasto-plasticity and ductile damage

In the following, the equations of a *coupled* model of elasto-plasticity and ductile damage are given based on the framework proposed by Lemaitre [2]. Small strains and rotations are assumed in the presentation, while in the numerical implementation large rotations are accounted for in the co-rotational elements.

The strain tensor $\boldsymbol{\varepsilon}$ is decomposed into elastic and plastic parts

$$\boldsymbol{\varepsilon} = \boldsymbol{\varepsilon}^{e} + \boldsymbol{\varepsilon}^{p} \tag{1}$$

where $\boldsymbol{\varepsilon}^{e}$ and $\boldsymbol{\varepsilon}^{p}$ are the elastic and plastic strain tensors, respectively. The relation between the stress tensor and the elastic strain tensor $\boldsymbol{\sigma}$ is defined as

$$\boldsymbol{\sigma} = \left(1 - D\right)\mathbf{C} : \boldsymbol{\varepsilon}^{e} \tag{2}$$

where $0 \le D < 1$ is the damage variable and $\mathbf{C}$ is the fourth order tensor of elastic constants. Isotropic elasticity is assumed, and $\mathbf{C}$ is therefore defined by Young's modulus $\mathbf{E}$ and Poisson's ratio ν.

According to the strain equivalence principle (Lemaitre [2]), the yield function is expressed in the form

$$f = \bar{f}\left(\frac{\boldsymbol{\sigma}}{1 - D}\right) - \left(\sigma_0 + R\right) \le 0 \tag{3}$$

where σ_0 is the yield stress, R is the strain hardening variable, while the convex function $\bar{f}$ is defined in the next section. The strain hardening is given by

$$R = \sum_{i=1}^{2} Q_i (1 - \exp(-C_i r)) \tag{4}$$

where r is the accumulated plastic strain and Q_i and C_i are strain hardening constants.

The associated flow rule defines the evolution of the plastic strain tensor and the accumulated plastic strain as

$$\dot{\boldsymbol{\varepsilon}}^{p} = \dot{\lambda} \frac{\partial f}{\partial \boldsymbol{\sigma}}; \quad \dot{r} = -\dot{\lambda} \frac{\partial f}{\partial R} \tag{5}$$

where $\dot{\lambda} \geq 0$ is the plastic multiplier. The damage evolution reads (Lemaitre [2])

$$\dot{D} = \begin{cases} 0 & \text{for} \quad r \leq r_D \\ \dot{\lambda} \dfrac{Y}{S(1-D)} & \text{for} \quad r > r_D \end{cases} \tag{6}$$

where r_D is the damage threshold, and Y is defined as

$$Y = \frac{1}{2} \boldsymbol{\varepsilon}^{e} : \mathbf{C} : \boldsymbol{\varepsilon}^{e} \tag{7}$$

The loading/unloading conditions are written in the Kuhn-Tucker form

$$f \leq 0; \quad \dot{\lambda} \geq 0; \quad \dot{\lambda} f = 0 \tag{8}$$

These equations are used to define plastic loading and elastic unloading, while the consistency condition, $\dot{\lambda}\dot{f} = 0$, is utilised to determine the plastic multiplier $\dot{\lambda}$ during a plastic process.

Yield criterion

The function $\bar{f}$ in the yield criterion of the model has yet to be determined. Since extruded aluminium alloys are textured materials, the anisotropic yield criterion *Yld96* of Barlat et al. [3] is adopted. The criterion is defined as

$$2\bar{f}^{m} = \alpha_1 |s_2 - s_3|^{m} + \alpha_2 |s_3 - s_1|^{m} + \alpha_3 |s_1 - s_2|^{m} \tag{9}$$

where s_1, s_2 and s_3 are the *principal*, deviatoric, equivalent isotropic stresses. These can be calculated having determined the deviatoric, equivalent isotropic stresses from the transformation

$$\mathbf{s} = \mathbf{L} : \boldsymbol{\sigma} \tag{10}$$

For plane stress states and with reference axes coincident with the axes of orthotropy, the matrix representation of the tensors in Eq. (10) is

$$\mathbf{s} = \begin{Bmatrix} s_x \\ s_y \\ s_z \\ s_{xy} \end{Bmatrix}, \quad \mathbf{L} = \frac{1}{3} \begin{bmatrix} c_2 + c_3 & -c_3 & -c_2 & 0 \\ -c_3 & c_3 + c_1 & -c_1 & 0 \\ -c_2 & -c_1 & c_1 + c_2 & 0 \\ 0 & 0 & 0 & 3c_6 \end{bmatrix} \quad \text{and} \quad \boldsymbol{\sigma} = \begin{Bmatrix} \sigma_x \\ \sigma_y \\ \sigma_z \\ \sigma_{xy} \end{Bmatrix} \tag{11}$$

where c_1, c_2, c_3 and c_6 are material parameters and $\sigma_z = 0$. Having determined s_x, s_y, s_z and s_{xy}, the corresponding principal stresses can be found according to a procedure proposed by Yoon et al. [4]. The **z**-axis is always a principal axis and may thus be assumed to coincide with the **3**-axis, so that

$$s_3 = s_z \tag{12}$$

The remaining principal stresses are determined from the well-known equations

$$\begin{matrix} s_1 \\ s_2 \end{matrix} = \frac{s_x + s_y}{2} \pm \sqrt{\left(\frac{s_x - s_y}{2} \right)^2 + s_{xy}^2} \tag{13}$$

while the angle θ between the **x**-axis and the **1**-axis is calculated as

$$\theta = \frac{1}{2} \arctan\left(\frac{2s_{xy}}{s_x - s_y} \right) \tag{14}$$

The coefficients α_1, α_2 and α_3 are finally given as

$$\begin{aligned} \alpha_1 &= \alpha_x \cos^2\theta + \alpha_y \sin^2\theta \\ \alpha_2 &= \alpha_x \sin^2\theta + \alpha_y \cos^2\theta \\ \alpha_3 &= \alpha_{z0} \cos^2 2\theta + \alpha_{z1} \sin^2 2\theta \end{aligned} \tag{15}$$

where α_x, α_y, α_{z0} and α_{z1} are material parameters. It is referred to Barlat et al. [3], Yoon et al. [4] and Lademo [5] for more details about the Yld96 criterion.

Numerical implementation and erosion criterion

The coupled model of elasto-plasticity and ductile damage has been implemented in LS-DYNA using a backward-Euler-type integration algorithm (Berstad et al. [6][7]; Lademo [5]). The model is implemented for co-rotational shell elements in plane stress. The shell elements have one-point integration in the plane and several integration points or layers through the thickness where the constitutive equations are evaluated. In the implementation, the out-of-plane shear stresses are treated elastically; i.e. only the in-plane stress components enter into the coupled constitutive model of elasto-plasticity and ductile damage. The thickness change of the shell can be accounted for in the simulations, and it is thus possible to represent (at least approximately) the thinning of the shell in a localised neck.

It is assumed that a macrocrack occurs in the material when the damage variable reaches a critical value D_C(Lemaitre [2]). A fracture criterion is thus defined as

$$D = D_C \tag{16}$$

where D_C for simplicity is considered as a material constant. Note that a refined fracture criterion has been proposed by Lemaitre [2] in which the critical damage is a function of the stress state of the material, based on the assumption that the amount of energy dissipated in damage growth at fracture is constant.

In the model, the fracture criterion is coupled with the erosion algorithm available in LS-DYNA. As the fracture criterion is reached in one layer of a shell element this layer becomes inactive; i.e. the stress components in the layer are all taken equal to zero. If the middle layer of the shell element becomes inactive, the element is removed from the finite element model. This means that it is, in principle, possible to follow the evolution of a “crack” through the structure. The fracture criterion is checked in all integration points in the structure for each time step throughout the loading process.

Identification of parameters

The identification of the parameters entering into the yield criterion and the strain-hardening rule is based on tension tests and pure bending tests, using a method proposed by Malo et al. [8]. The resulting yield surface for aluminium alloy AA7108 in temper T1 is presented in Figure 1 (Lademo [5]), where the strong anisotropy of this alloy is clearly demonstrated. The AA7108 alloy is used for instance in car bumpers. The yield stress for balanced biaxial stress conditions was not determined experimentally, making the shape of the yield surface uncertain in this region of the stress space. The yield strength and initial values of the strain hardening constants are determined based on tension tests in the extrusion direction. The material constants for AA7108-T1 are compiled in Table 1.

The damage parameters may be determined by one of several methods proposed by Lemaitre and Chaboche [9]. In this study, the method based on *variation of plasticity characteristics* is combined with inverse modelling of tension tests to obtain proper values of r_D, S and D_C. The damage threshold parameter, r_D, was assumed to be equal to zero in order to simplify the identification process. Then, only two parameters are left to identify; that controls the evolution of the damage, and D_C that controls when the failure occurs.

The finite element model of the test specimen is shown in Figure 2. The deformation is defined by prescribing the velocity of two bolts through the specimen's extremities. The bolts were modelled as a quarter of a circle consisting of shell elements made of rigid material. In order to avoid contact problems, adjacent material in the bolts and test specimen has been connected node to node. The finite element model consists of 2760 Belytschko-Tsay membrane elements with one point integration in the plane and through the thickness. The deformation that led to failure of the specimens was applied during 7-8 ms depending of the ductility of the test specimen. The total kinetic energy and the change of the kinetic energy were small compared to the total energy of the system in all simulations. Consequently, dynamic effects are probably small so that the response can be considered quasi-static.

Ideally, the parameter S should be determined first. The idea was to determine the damage parameters so that the post necking behaviour was correctly described for the different curves. Considerations based on test data and some trial-and-error analyses led to the choice , which gave approximately 3 % of damage at 15 % of strain. Damage lowers the strength of the material, but this was not taken into account when determining initial values of the hardening parameters from the uniaxial tensile tests. Therefore, after choosing the parameter S, the hardening parameters were slightly changed. Finally, D_C should ideally be determined so that failure occurs at the correct displacement. The choice D_C gave the force-displacement curves shown in Figure 3(a). The abrupt failure observed in the experiment in the 0°-direction is not predicted in the numerical analyses. Furthermore, the hardening in the 90°-direction is too high and diffuse necking and failure are delayed. Some deviations are also seen in the 45°-direction for large displacements.

Numerical study

Effect of mesh density

The damage evolution leads to strain softening when the strain reaches a certain level depending on the stress triaxiality of the stress state. It follows that the finite element results may become severely mesh dependent due to strain localisation. There exists several regularisation methods to deal with this problem, e.g. non-local regularisation or regularisation by including rate dependence in the constitutive model (Belytschko et al. [10]).

In this study, no regularisation method has yet been implemented, but the non-local regularisation will be adopted in further work. In order to check the influence of the mesh density on the computed results, the tensile tests were simulated with three different meshes: a coarse mesh, a fine mesh and an adaptive mesh. The coarse mesh is shown in Figure 2, while the number of elements is doubled in both directions in the fine mesh. The adaptive mesh is equal to the coarse mesh initially and is then refined according to a damage-driven fission-based adaptive procedure, which is currently under development. The maximum number of refinement levels was three in all simulations.

The results are presented in Figure 3(b). It is seen that the mesh sensitivity of the force-displacement curves is only moderate for the current, limited range of mesh densities. The failure modes observed in the experiments and the various simulations are compared in Figure 4 to Figure 6. The agreement obtained between the experimental and numerical failure modes is quite good, and in particular the influence of anisotropy is well predicted. Furthermore, it is seen that the failure modes are similar for the coarse, fine and adaptive meshes.

Biaxial tensile tests

Numerical simulations of biaxial tensile tests on cruciform specimens were used in an attempt to assess the validity of the material model. The finite element model is shown in Figure 7. The complete model consists of 10796 shell elements with one point integration in the plane and two layers through the thickness. The size of the elements in the gauge section is similar to the element size in the fine mesh used for the uniaxial test specimens. The outermost parts of the extremities were modelled as rigid, while the remaining parts were assumed to be elastic, since the extremities are six times thicker than the gauge section.

In the experiments, the force was applied to the extremities of the specimen through bolts, while the specimens were loaded by prescribing the velocities of the extremities in the simulations. Various proportional loading paths were investigated both experimentally and numerically (Lademo [5]). It was checked that the total kinetic energy and the change of the kinetic energy were small compared to the total energy of the system in all simulations, and thus the response can be considered to be quasi-static.

Figure 8 compares the failure mode observed in one experiment with strain ratio $\varepsilon_2/\varepsilon_1 = 1$ against the predicted response using LS-DYNA. Qualitatively, good agreement is observed in this experiment. Reasonably good results were obtained also for other strain ratios.

Concluding remarks

A coupled model of elasto-plasticity and ductile damage was implemented for co-rotational shell elements in the non-linear explicit finite element code LS-DYNA using a backward-Euler algorithm. Critical damage is used as erosion criterion. The model includes the anisotropic yield criterion Yld96 proposed by Barlat and co-workers, which was found to be superior with respect to accuracy for the actual aluminium alloys.

Numerical simulations of tension tests with specimens purpose-made for identification of damage parameters showed that quite good agreement between the observed behaviour and predictions could be obtained. Finally, the material model was used to study failure of a cruciform specimen loaded in biaxial tension. The failure mode observed in the experiment was reasonably well predicted in the simulation.

Acknowledgement

The support of the Norwegian Research Council and Hydro Automotive Structures AS is gratefully acknowledged.

References

[1] LS-DYNA (1997). “Keyword User’s Manual”, Livermore Software Technology Corporation, Version 940.

[2] Lemaitre, J. (1992). “A Course on Damage Mechanics“, Springer-Verlag.

[3] Barlat, F., Maeda, Y., Chung, K., Yanagawa, M., Brem, J.C., Hayashida, Y., Lege, D.J., Matsui, K., Murtha, S.J., Hattori, S., Becker, R.C. Makosey, S. (1997). “Yield Function Development for Aluminum Alloy Sheets”, J. Mech. Phys. Solids, 45, pp. 1727-1763.

[4] Yoon, J.W., Barlat, F., Chung, K., Pourboghrat, F., Yang, D.Y. (1998). “Influence of initial back stress on the earing prediction of drawn cups for planar anisotropic aluminium sheets”, Journal of Materials Processing Technology, 80-81, pp. 433-437.

[5] Lademo, O.-G., (1999). “Engineering Models of Elastoplasticity and Fracture for Aluminium Alloys“, Dr.ing. thesis 1999:39, Department of Structural Engineering, Norwegian University of Science and Technology, Trondheim, Norway.

[6] Berstad, T., Hopperstad, O. S and Langseth, M. (1994). “Elasto-Viscoplastic Constitutive Models in the Explicit Finite Element Code LS-DYNA3D”, Second International LS-DYNA3D Conference, San Francisco, Sept. 20-21.

[7] Berstad, T., Hopperstad, O.S., Lademo, O.-G. and Malo, K.A. (1999). “Computational model of ductile damage and fracture in shell analysis“, Second European LS-DYNA Conference, Gothenburg, June 14-15.

[8] Malo, K.A., Hopperstad, O.S., Lademo, O.-G. (1998). “Calibration of anisotropic yield criteria using uniaxial tension tests and bending tests”, Journal of Materials Processing Technology, 80-81, pp. 538-544.

[9] Lemaitre, J., Chaboche, J.-L. (1990), “Mechanics of Solid Materials”, Cambridge University Press.

[10] Belytschko, T., Liu, W.K. and Moran, M. (2000), “Nonlinear Finite Elements for Continua and Structures”, Wiley.

Material constants for the coupled model of elasto-plasticity and damage for aluminium alloy AA7108 in temper T1

Yield criterion		Elasticity & strain hardening		Damage evolution	
Parameter	Value	Parameter	Value	Parameter	Value
m	8	E [MPa]	70000	r_D	0.0
c_1	1.254	ν	0.31	S [MPa]	10
c_2	0.700	σ_0 [MPa]	320	D_C	0.15
c_3	1.012	Q_1 [MPa]	37.8		
c_6	0.935	C_1	471.6		
α_x	0.188	Q_2 [MPa]	373.5		
α_y	8.843	C_2	6.905		
α_{z0}	1.000				
α_{z1}	10.19				

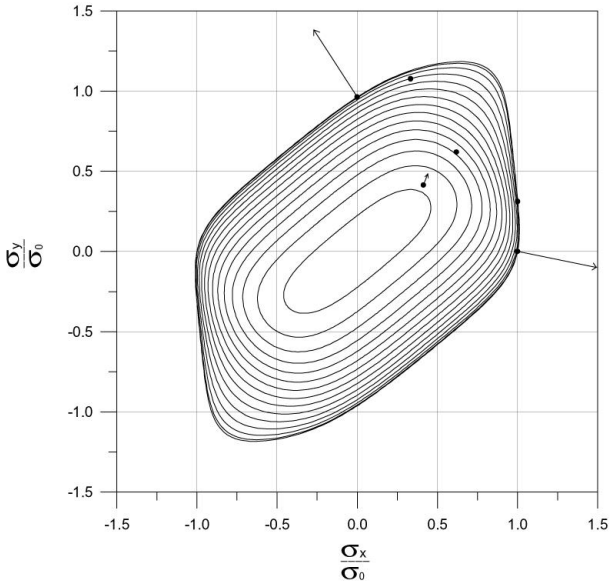

Figure 1 'Yld96' criterion for AA7108-T1. Black dots indicate measured yield stresses, whereas the arrows represent measured R-ratios. The contours represent levels of constant normalised shear stress.

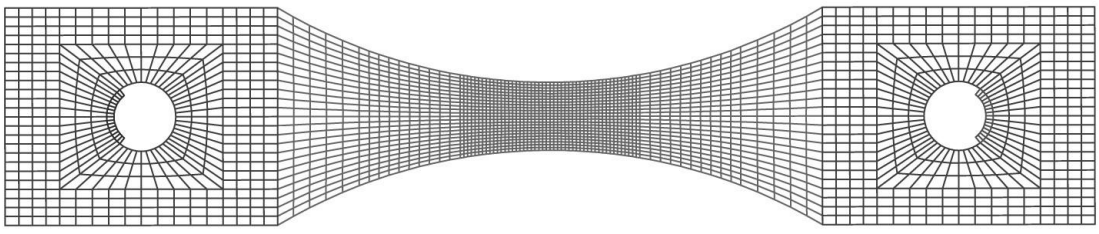

Figure 2 FE-model of the test specimen for damage identification.

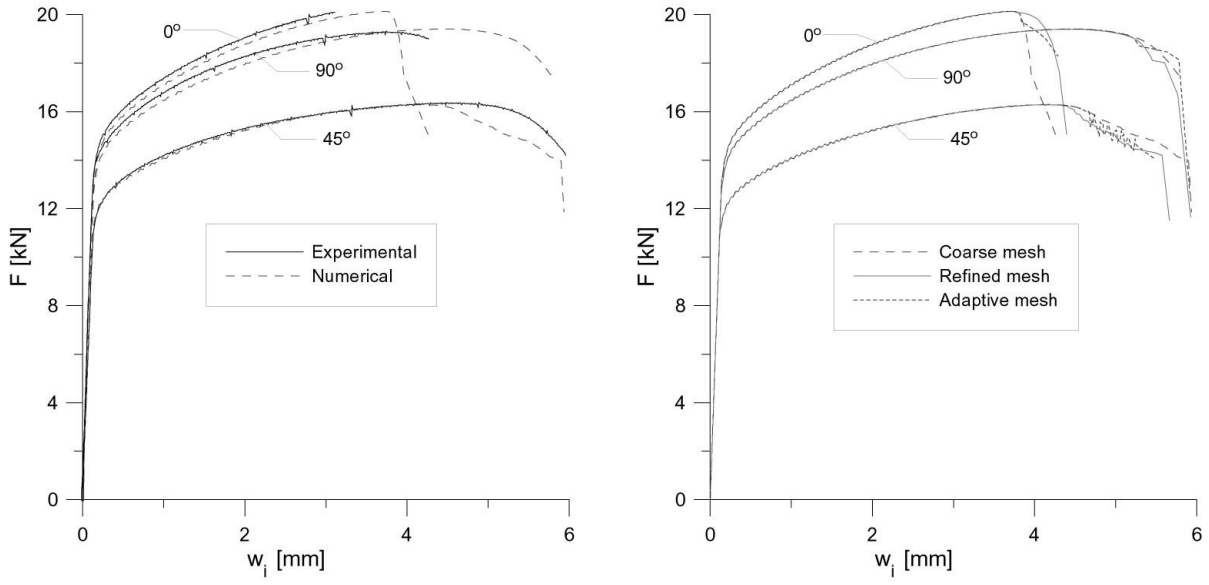

a) b)

Figure 3 Force against deformation of the inner 33 mm of the test specimens for damage identification. (a) Experiments and numerical simulations with the coarse mesh. (b) Numerical simulations with coarse, fine and adaptive meshes.

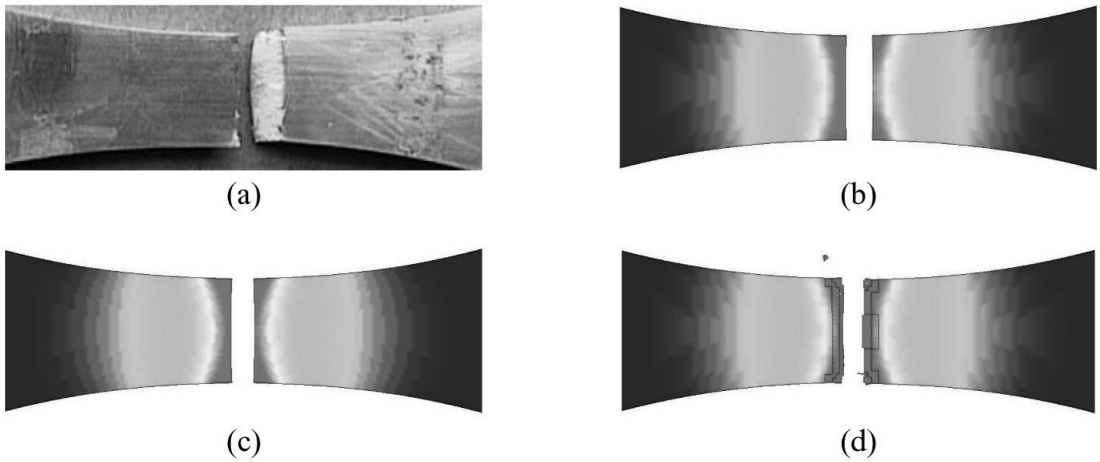

Figure 4 Failure of test specimen in 0°-direction: (a) experimental, (b) coarse mesh, (c) fine mesh and (d) adaptive mesh.

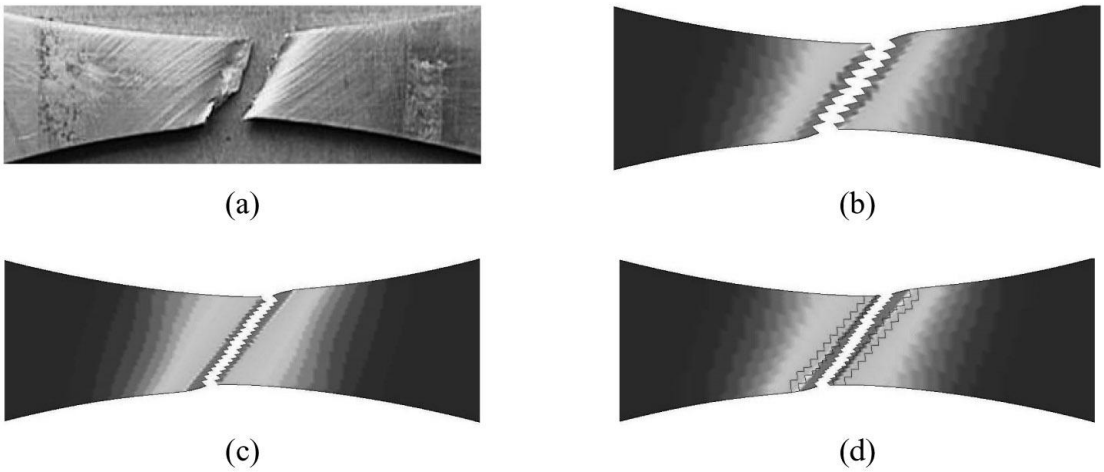

Figure 5 Failure of test specimen in 45°-direction: (a) experimental, (b) coarse mesh, (c) fine mesh and (d) adaptive mesh.

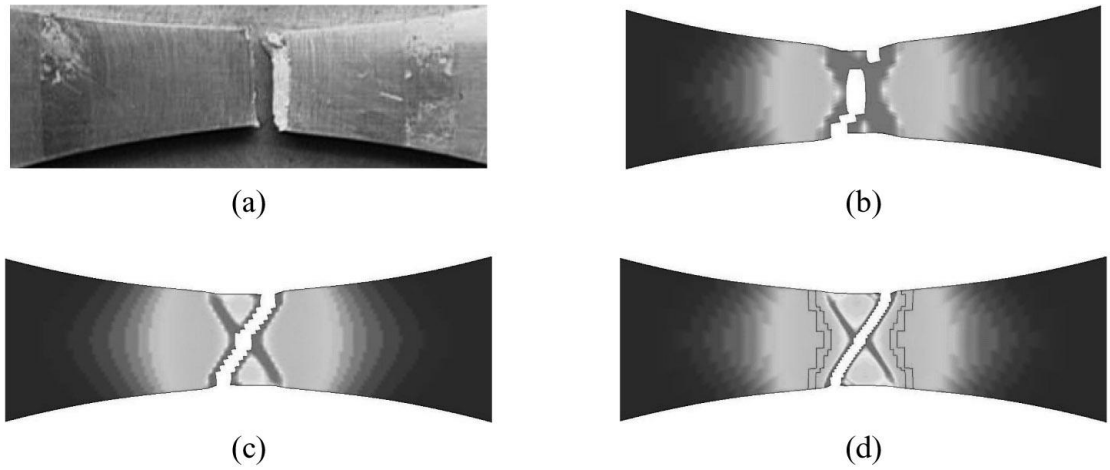

Figure 6 Failure of test specimen in 90°-direction: (a) experimental, (b) coarse mesh, (c) fine mesh and (d) adaptive mesh.

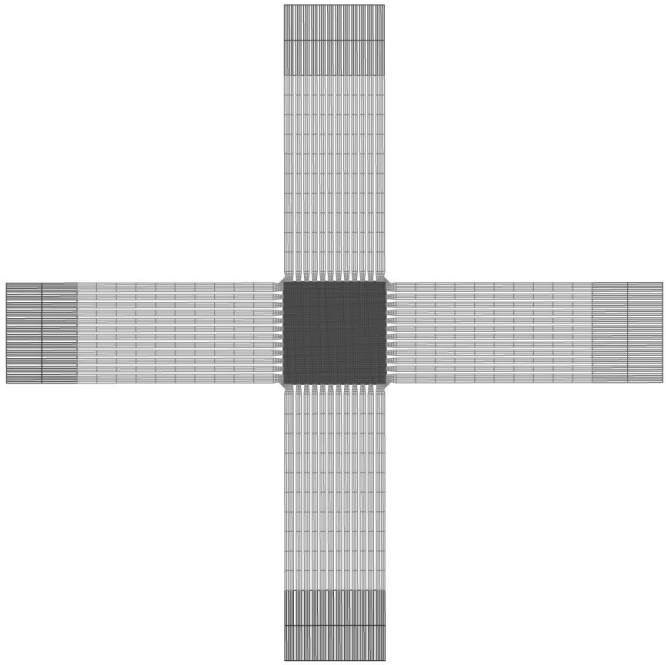

Figure 7 Finite element mesh of cruciform test specimen modelled with shell elements.

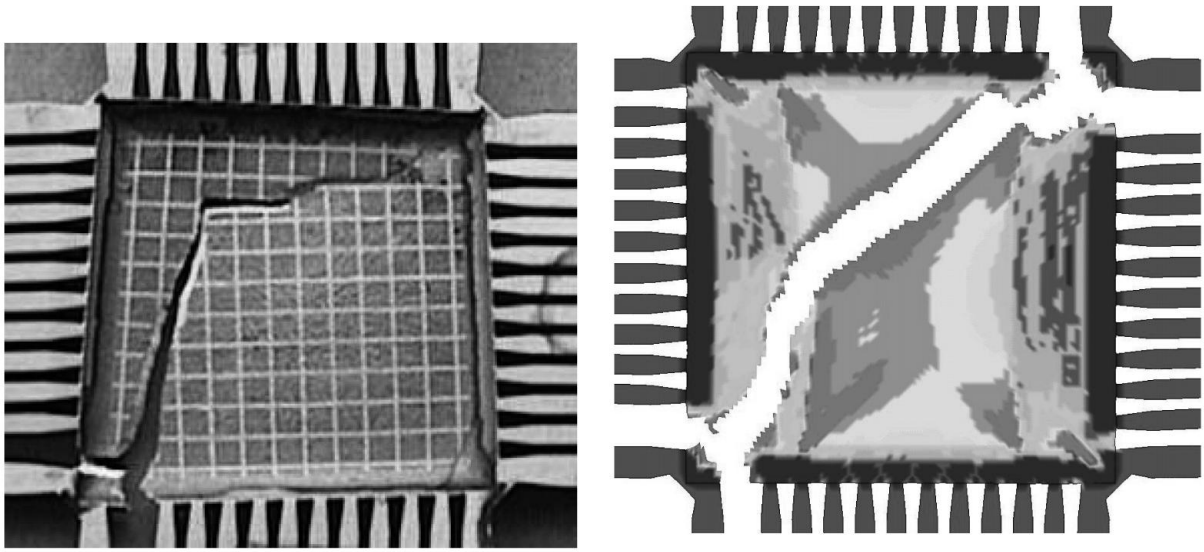

Figure 8 Failure mode of biaxial test with strain ratio $\varepsilon_2/\varepsilon_1 = 1$: (a) experiment and (b) numerical simulation.